Characterizing Wettability Using ^{13}C Magnetic Resonance Relaxation Times

Naser Ansaribaranghar[1,2], *Mohammad Sadegh* Zamiri[1], *Fabrice* Pairoys[3], *Victor* Fernandes[3], *Laura* Romero-Zerón[2], *Florea* Marica[1], *Andres* Ramirez Aguilera[1], *Derrick* Green[4], *Benjamin* Nicot[3], *and Bruce J.* Balcom[1,*]

[1]UNB MRI Centre, Department of Physics, University of New Brunswick, Fredericton, New Brunswick E3B 5A3, Canada
[2]Department of Chemical Engineering, University of New Brunswick, Fredericton, New Brunswick E3B 5A3, Canada
[3]TotalEnergies, Avenue Larribau, 64000 Pau, France
[4]Green Imaging Technologies, Fredericton, New Brunswick E3A 8V2, Canada

Abstract. Wettability is a crucial parameter in the petroleum industry and influences factors, such as flow (relative permeability), fluid distribution (residual oil saturation, capillary pressure), hydrocarbon recovery, and fluid connectivity. The accurate determination of rock wettability is essential for optimizing production strategies and maximizing resource recovery. Traditional methods for assessing rock wettability, such as the USBM and Amott methods, are labor-intensive and time-consuming. In contrast, Magnetic Resonance (MR) offers a noninvasive approach to probe fluid saturated core plugs, providing valuable insights into rock wettability without the need for extensive sample preparation. MR parameters such as T_1, T_2, and D and their correlations are sensitive to fluid-rock (surface) interactions, making them promising candidates for rock wettability determination. While ^1H MR can suffer from signal overlap between oil and brine, ^{13}C MR presents a novel solution in petrophysics and core analysis to overcome this limitation by measuring only hydrocarbons. In this study, we focused on the use of ^{13}C MR relaxation times as a tool for understanding pore surface wettability. By comparing aged rock samples with different wettabilities, we demonstrated the application of ^{13}C MR relaxation times in characterizing pore-surface interactions and wettabilities. These findings highlight the potential of ^{13}C MR as a tool for rock wettability assessments in the petroleum industry. Implementing these non-invasive methods in routine core analysis will advance SCAL wettability determination, offering a rapid and efficient means to obtain essential rock wettability information for reservoir characterization and production optimization.

1 Introduction

Wettability is a crucial parameter in petroleum engineering for efficient oil recovery [1]. Wettability is important in other fields with many potential applications for example in material science for developing self-cleaning surfaces [2], biomedical engineering for designing medical implants [3], and environmental science for understanding soil-water interactions [4].

In the field of petroleum engineering, determining the wettability of core plugs is a critical factor that significantly influences fluid flow behavior [5], fluid distribution [6–8], and hydrocarbon recovery from petroleum reservoirs [9,10].

Magnetic Resonance (MR) is a noninvasive method that is sensitive to surface interactions. To assess the wettability of core plugs, various ^1H MR methods have been utilized, which are based on three main MR parameters: longitudinal relaxation time T_1, transverse relaxation time T_2, and diffusivity D. A review of the advantages and disadvantages of different MR methods to determine core plug wettability was presented by Valori et al. [11,12]. The issue of oil/water signal overlap poses a significant drawback in all ^1H MR methods. Because of this problem, previous studies have predominantly relied on unrealistic fluids, which limits their applicability to realistic samples. Although several attempts have been made to overcome this issue, a comprehensive answer using a simple approach has not been suggested.

This study introduces a novel method utilizing ^{13}C MR techniques to evaluate the wettability of core plugs. Because ^{13}C is unique to oils, it is not necessary to distinguish between water and oil signals [13,14]. Our study shows, for the first time, a reliable sensitivity of the ^{13}C relaxation times to rock and fluid interactions and different wettability conditions. This is proven by exploring realistic samples. The ^{13}C T_2 relaxation time and T_1/T_2 ratio of various core plugs with different wettability, saturated with realistic fluids (crude oil and brine) were studied.

Common industry tests like the Amott-Harvey and U.S. Bureau of Mines (USBM) test [15–17], exhibit limitations in determining core plug wettability. Challenges include difficulty in restoring plugs after

* Corresponding author: bjb@unb.ca

cycling [18], leading to biased EOR agent assessments and non-uniform wettability distribution. The complex process of wettability alteration, influenced by surfactant adsorption and nanofluid injections, reinforces the need for a new analytical approach [19,20][21–24].

By innovatively employing ^{13}C MR techniques, this study not only overcomes the limitations of current MR methods and industry standards but also paves the way for a more accurate and nuanced understanding of wettability within core plugs. Such advancements have the potential to significantly enhance the reliability and efficiency of petrophysical studies and Special Core Analysis Laboratories (SCAL) tests.

In what follows, we delve into a detailed methodology outlining our novel approach, present a comparative analysis against traditional methods, and discuss the broader impacts of our findings on advancing wettability assessment techniques in petroleum engineering and related fields.

2 Materials and methods

Aged core plugs were studied to show the application of the proposed method to realistic samples. We used 6 Bentheimer core plugs that were prepared and tested for their Amott index by Pairoys et al. (2023) [25] as part of a larger study on the effect of dopant at different concentrations on the oil recovery. The samples were initially saturated with undoped or doped brines, brought to irreducible water saturation (S_{wi}) and aged using crude oil at reservoir temperature. The samples were then loaded in Amott cells for spontaneous imbibition before being brought to residual oil saturation (S_{or}) during centrifuge forced imbibition. The rock and fluid properties, procedure and results of drainage, aging, spontaneous imbibition, and forced imbibition are described in detail by Pairoys et al. (2023) [25]. A summary of the sample properties and their status is outlined in the following sections.

2.1 Rock and fluid properties

The 6 core plugs were prepared as follows: sample # 1, which was called Reference test, and samples # 2 and # 3 were prepared to see the impact of sodium iodide, NaI, in imbibing brine only. Samples # 4, # 5, and # 6 were prepared to see the impact of NaI concentration in initial sitting brine (initial saturating brine). In the following, a description of the samples is provided. A summary of the connate brine and imbibing brine for each sample is tabulated in Table 2. Sample #1 (Be1): Bentheimer sandstone rock with Middle Eastern oil and connate brine containing no sodium iodide. Imbibition was conducted with connate brine containing no iodide. Sample #2 (Be2): Bentheimer sandstone rock with Middle Eastern oil and connate brine containing no iodide. Imbibition was performed by employing imbibing brine containing 1g/l of NaI. Sample #3 (Be3): Bentheimer sandstone rock with Middle Eastern oil and connate brine containing no Iodide. Imbibition was carried out using imbibing brine containing 12g/l of NaI. Sample #4 (Be4): Bentheimer sandstone rock with Middle Eastern oil and connate brine containing 1g/l of NaI. Imbibition was conducted by imbibing brine containing 1g/l of NaI. Sample #5 (Be5): Bentheimer sandstone rock with Middle Eastern oil and connate brine containing 6g/l of NaI. Imbibition was performed with imbibing brine containing 6g/l of NaI. Sample #6 (Be6): Bentheimer sandstone rock with Middle Eastern oil and connate brine containing 12g/l of NaI. Imbibition was carried out with connate brine containing 12g/l of NaI. Table 1 and Table 2 provide information on the compositions of the initial "connate" brines as well as the brines involved in imbibition, including spontaneous imbibition (SPI) and forced imbibition (FI). SW*1 means that 1 g/l of NaI was added to the SW* brine.

Table 1. Brine compositions.

Salt	SW* C [g/l]	SW*1 C [g/l]	SW*6 C [g/l]	SW*12 C [g/l]
NaCl	26.8	26.8	24.8	225
KCl	0.96	0.96	0.96	0.96
CaCl2, 2H2O	3	3	3	3
MgCl2, 6H2O	12.4	12.4	12.4	12.4
NaI	0	1	6	12

Table 2. Symbols of connate brine and imbibing brines per sample test.

Sample ID	Brine at S_{wi}	SPI and FI brine
Be1	SW*	SW*
Be2	SW*	SW*1
Be3	SW*	SW*12
Be4	SW*1	SW*1
Be5	SW*6	SW*6
Be6	SW*12	SW*12

Based on sample preparations, the samples can be grouped into pairs. Samples #3 and #6 were compared together because they have the same flooding brine, but different initial brine. Another pair were samples #2 and #4 were. The next pair were samples #1 and #5 because in sample # 1 iodine was not introduced, while in sample # 5 iodine was introduced in both the initial saturating brine and the imbibing brine. Also, from another point of view, samples #1, #2, and #3 can be grouped as one set because these samples did not contained iodine in the connate brine, while a second set consisted of samples #4, #5 and #6 because these samples were initially saturated with brine containing iodine.

2.2 MR measurements

^{13}C and ^{1}H MR experiments were undertaken to obtain T_2, as well as T_1-T_2 relaxation correlations. Two-dimensional T_1-T_2 correlations were obtained using the Inversion-

Recovery-CPMG sequence. Details of the T_1-T_2 measurement can be found elsewhere [26–28]. The IR-CPMG pulse sequence, Figure 1, begins with a 180° pulse, then after an inversion time t_{int}, a 90° pulse is applied followed by a series of 180° pulses to acquire a CPMG echo train. The signal equation is described by:

$$S(t, t_{int}) = \iint dT_1 dT_2 f(T_1, T_2)(1 - 2\exp\{-t_{int}/T_1\})\exp\{-t/T_2\} \quad (1)$$

where f (T_1, T_2) is the T_1-T_2 distribution function, t is the cumulative echo time starting at the 90° pulse while t_{int} is the recovery time between the inverting 180° pulse and the subsequent 90° pulse of the CPMG measurement. Data analysis involves a 2D Laplace inversion to extract f (T_1, T_2) from the measured set of echo amplitudes S (t, t_{int}).

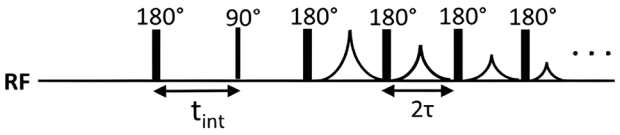

Fig. 1 IR-CPMG pulse sequence [29].

The 90° and 180° rf pulse durations for ^{13}C measurements were t_{90}= 42.62 μs and t_{180} = 76.76 μs, respectively. T_2 relaxation times were determined using the standard CPMG experiment [30,31]. In ^{13}C measurements the temporal separation of spin echoes was t_e = 1000 μs. A total of 64 data points were acquired at the top of each spin echo with a dwell time of t_{dw} = 10 μs. The duration of each CPMG decay was 2 s and 2000 echoes were recorded. A recycle delay of t_{RD} = 30 s was included between each scan, and 512 repeat scans were summed. Two-dimensional T_1-T_2 correlations were obtained using the Inversion-Recovery-CPMG sequence [28,32]. In ^{13}C measurements the T_1 recovery interval was varied logarithmically from τ_1 = 105 μs to 25 s over 40 separate acquisitions. The CPMG echo time was fixed at t_e = 1000 μs, with all other parameters equal to those given above. A recycle delay of t_{RD} = 30 s was included between each scan, and 32 repeat scans were summed.

The 90° and 180° rf pulse durations for ^{1}H measurements were t_{90}= 10.10 μs and t_{180} = 20.85 μs, respectively. In ^{1}H CPMG experiments the echo time was t_e = 1000 μs. A total of 9 data points were acquired at the top of each spin echo with a dwell time of t_{dw} = 10 μs. The duration of each CPMG decay was 2 s with 2000 echoes recorded. A recycle delay of t_{RD} = 15 s was included between each scan, and 32 repeat scans were summed. In the ^{1}H Inversion-Recovery-CPMG experiments, the T_1 recovery interval was varied logarithmically from τ_1 = 60.6 μs to 3 s over 30 separate acquisitions. The CPMG echo time was fixed at t_e = 1000 μs, with all other parameters equal to those given above. A recycle delay of t_{RD} = 15 s was included between each scan, and 2 repeat scans were summed.

2.3 MR instruments

^{13}C and ^{1}H measurements were acquired using a variable field Cryogen Free Superconducting magnet (MR Solutions, Guildford, Surrey, UK) at 3.1 T for ^{13}C and 0.79 T for ^{1}H both with a resonance frequency of 33.7 MHz. The RF probe was a homemade birdcage. The magnet is permanently connected to a magnet power supply (Cryomagnetics, Inc., TN, US). GIT system software (Green Imaging Technologies, Inc., NB, Canada) was employed to execute CPMG and IR-CPMG measurements.

2.4 Processing

An in-house MATLAB script was used to process the data. A Fast Laplace Inversion algorithm (Laplace Inversion Software, Schlumberger-Doll Research) written in MATLAB (MathWorks, Natick, MA) was used to produce the T_2 distributions and T_1-T_2 relaxation correlations.

2.5 Theory

^{13}C is an MR sensitive nucleus with 1.1% natural abundance, and its gyromagnetic ratio (γ) is four times lower than that of ^{1}H. ^{13}C has low sensitivity due to low natural abundance and low gamma, but relaxation mechanism for ^{13}C should be the same as for ^{1}H since both are spin 1/2.

MR parameters (T_1, T_2, D, and their correlations) are widely accepted to be sensitive to fluid-rock (surface) interactions. Therefore, each of these parameters can be used to extract wettability. Among these parameters, T_2 is the most used parameter for wettability assessment. A simplistic model of spin relaxation within a single pore describes the measured relaxation time as the weighted average of surface and bulk relaxing spins, such that [33]:

$$\frac{1}{T_{1,2}} = \frac{1}{T_{1,2,surf}} + \frac{1}{T_{1,2,bulk}} \quad (2)$$

$$\frac{1}{T_{1,2}} = \rho_{1,2}\frac{S}{V} + \frac{1}{T_{1,2,bulk}} \quad (3)$$

where $1/T_{1,2}$ is relaxation time, $1/T_{1,2,surf}$ is the surface relaxation component, $1/T_{T_{1,2,bulk}}$ is the bulk relaxation component, ρ is the surface relaxivity term and S/V is the surface-to-volume ratio.

The T_2 method is based on the fact that the interaction between fluids and the pore surface decreases the observed T_2 value [34,35]. The main advantage of this method is that T_2 measurement is straightforward and rapid. However, it is dependent on pore size distribution and saturation.

One approach to solve this problem is to use the T_1/T_2 relaxation correlation ratio [11,12,36–38] to better isolate the effect of surface interactions from pore size and saturation of fluids. The following equation can be derived from Eq. 2 by assuming $T_{1,\,bulk}$=$T_{2,\,bulk}$=T_b [11]:

$$\frac{T_1}{T_2} = \frac{T_{1s}\,[T_{2s} + T_b]}{T_{2s}\,[T_{1s} + T_b]} \quad (4)$$

This means that for fixed values of T_{1s}/T_{2s} and T_b the observed T_1/T_2 ratio is not fixed [11]. Figure 2 shows this fact for different combinations of T_b and T_{1s}/T_{2s}.

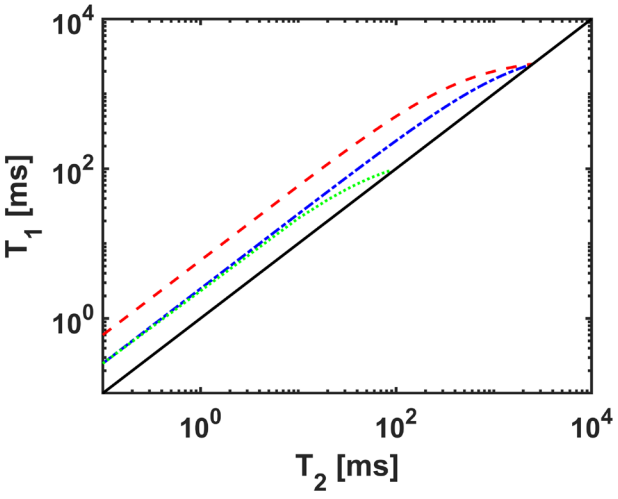

Fig. 2. Observed T_1/T_2 ratio for fixed bulk relaxation T_b and ratio between the surface components of the relaxation (T_{1s}/T_{2s}). Reproduced from the original plot from [11]. (– – –) refers to the (T_{1s}/T_{2s}) = 6 and T_b = 2.5 s. (– - –) refers to the (T_{1s}/T_{2s}) = 2.5 and T_b = 2.5 s. (…) refers to the (T_{1s}/T_{2s}) = 2.5 and T_b = 0.1 s. The solid line refers to the equal T_1 and T_2.

It should be noted that saturation does not change the shape of the plot, but it changes the location of the point on the line. This means that depending on the oil saturation, when T_1 and T_2 approach the bulk value the data do not contain any information on surface interactions and therefore extracting wettability will not be possible [11]. Ignoring this fact can lead to an incorrect interpretation of data. For example, if we have an oil wet sample with high T_1/T_2, then increasing saturation can shift the T_1/T_2 to bulk T_1 and T_2, and lower T_1/T_2 that could be interpreted as less oil wet or water wet sample. This misinterpretation can be easily prevented if we plot similar lines as above and compare the T_1/T_2 on it. Also, it should be noted that based on Figure 2 the diagonal shift of the straight line is only possible when there is a change in T_{1s}/T_{2s} which is directly related to wettability. Otherwise, the change in saturation and/or bulk effects might create the shifted T_1/T_2.

In this paper ^{1}H and ^{13}C T_2 and T_1-T_2 relaxation correlation are employed. We prove that ^{13}C is sensitive to wettability and surface interactions and oil wet conditions cause ^{13}C T_2 to decrease and ^{13}C T_1/T_2 to increase. The great advantage of the new approach is that it is not necessary to differentiate between phases and it also works with complex fluids. ^{1}H MR data showed signal overlap hence limited qualitative analysis could be done based on ^{1}H MR data.

3 Results and discussion

3.1 ^{13}C measurements

Fig. 3 shows the ^{13}C T_2 distribution for all the samples. The samples with no iodine in the initial brine (Be1, Be2, and Be3) show shorter T_{2LM} shown in Figure 4. These samples are reported as more oil wet with respect to the other 3 samples. This shift in ^{13}C T_2 distribution with respect to reference oil and between oil wet and less oil wet samples is a clear sign that ^{13}C is sensitive to rock and fluid surface interactions specifically wettability. Although there is a possibility that this difference in T_{2LM} might be due to differences in saturation, we will show later with ^{13}C T_1-T_2 that it is not the case.

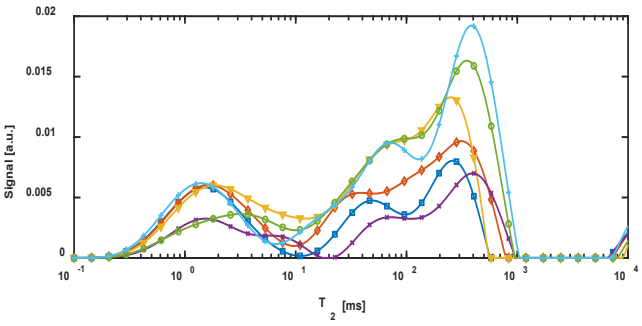

Fig. 3. ^{13}C T_2 distribution for core plugs in realistic system. (+) is for Be6, ○ is for Be5, * is for Be4, ◇ is for Be2, ▼ is for Be3, and ■ is for Be1.

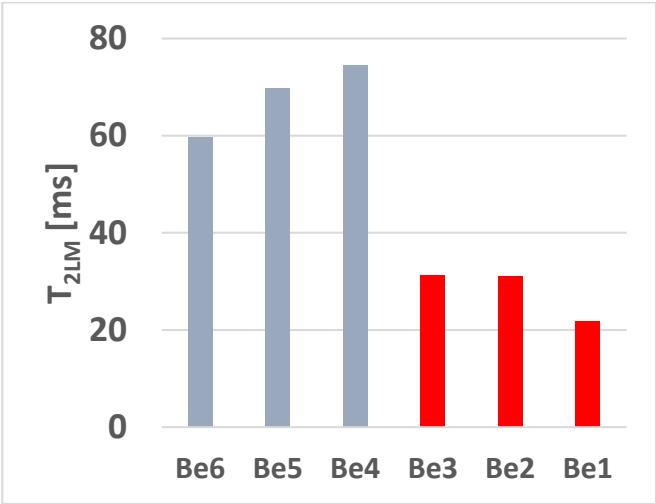

Fig. 4. ^{13}C T_{2LM} histograms were obtained from ^{13}C T_2 distribution of the samples.

Figure 5 presents ^{13}C T_1-T_2 relaxation correlation for all the samples. Clearly there is a shift towards higher T_1/T_2 for the samples with oil wet characteristics (Be1, Be2, and Be3). Also, less oil wet samples have lower T_1/T_2 which is a characteristic of water wet samples (Be4, Be5, and Be6).

Figure 6 shows the ^{13}C T_1/T_2 of the main peaks in T_1-T_2 relaxation correlations. Samples with oil wet characteristics (Be1, Be2 and Be3) have T_1/T_2 higher than 4 and samples with water wet characteristics (Be4, Be5 and Be6) have T_1/T_2 close to 2. It should be noted that for the reference oil T_1/T_2 was 1. This is in full agreement with the results obtained by Amott index measurements shown in Figure 7

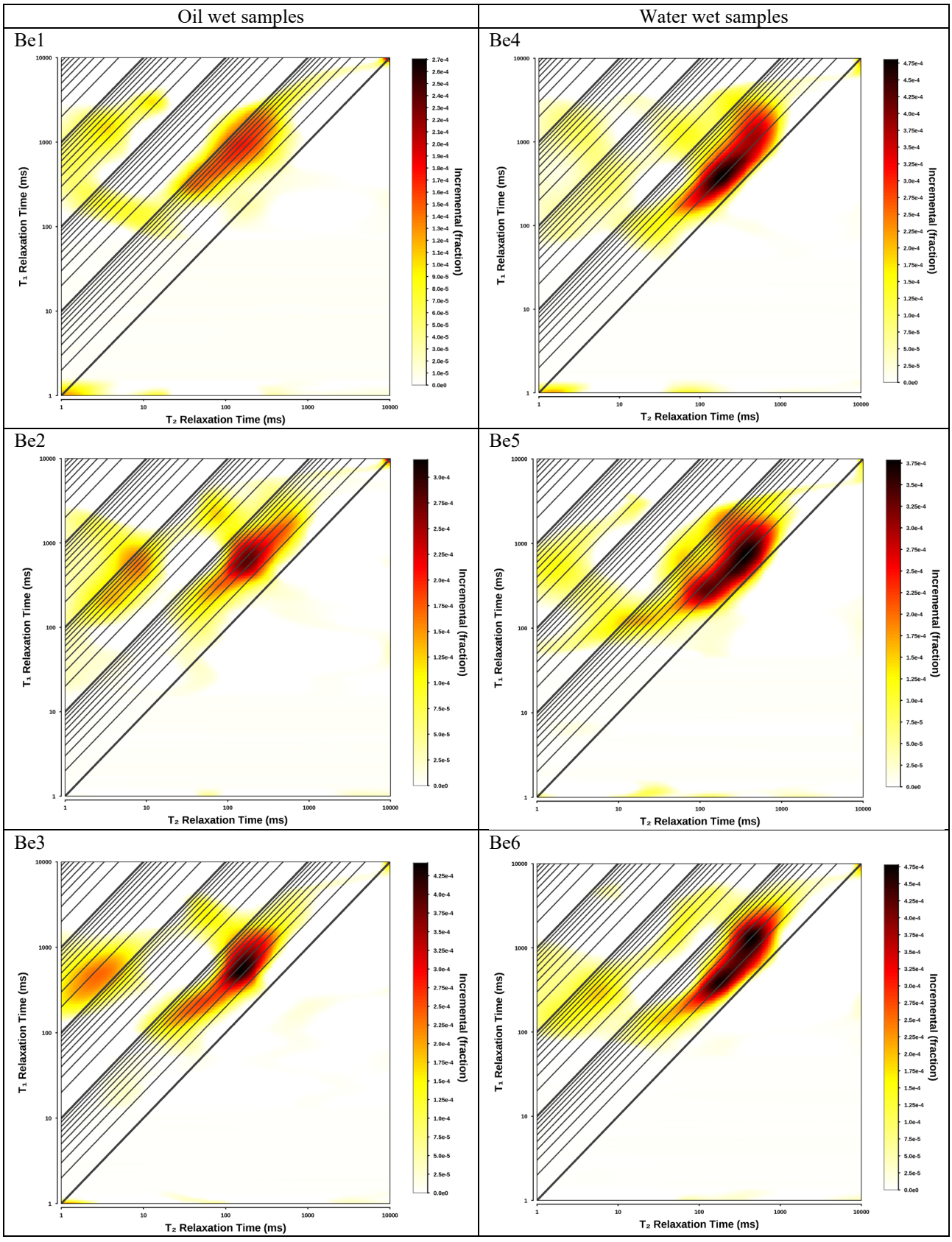

Fig. 5. ^{13}C T_1-T_2 relaxation correlation for realistic samples.

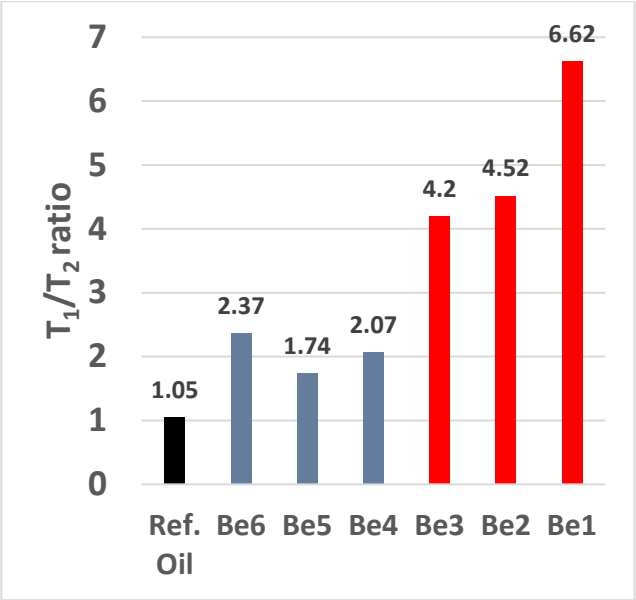

Fig. 6. ^{13}C T_1/T_2 ratio for the core plugs.

Based on the spontaneous displacement and forced imbibition saturation ranges, the Amott water wettability index *I*w can be calculated. Figure 7 shows the *I*w results for each sample. As stated in the original paper [25], this plot is probably the most relevant indication of the effect of NaI doping agent on wettability: all the rock samples without NaI in the sitting brine, and despite the doped imbibing brine, have similar *I*w ranging from 0.13 to 0.23. For the samples containing NaI in the sitting brines, *I*w values are much higher ranging from 0.44 to 0.74. It is important to note that at concentration of NaI of 1g/l in the connate brine (Be4), the *I*w value is double compared to the *I*w values of the tests without NaI in the connate brine (Be1, Be2, Be3). The same behavior was observed based on ^{13}C T_{2LM} and ^{13}C T_1/T_2.

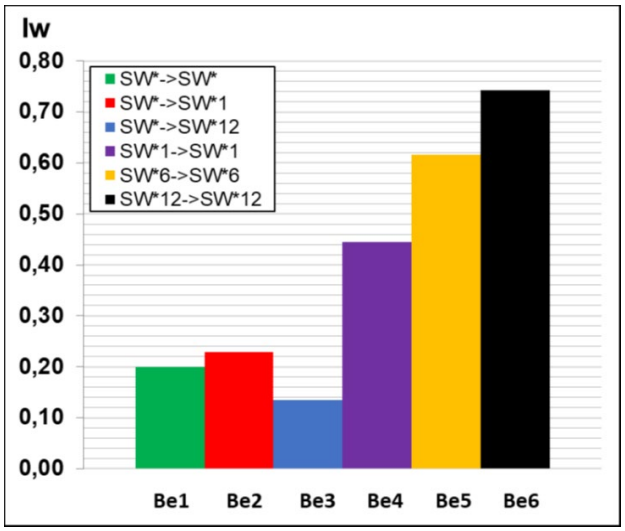

Fig. 7. Amott *I*w histograms [25].

By integrating the 2D spectrum of ^{13}C T_1-T_2 relaxation correlations [26], the distribution of the T_1/T_2 ratio can be determined. Figure 8 shows the test results for sample Be1, sample Be6, and the reference oil. Two dominant peaks are visible for the core plugs. The peaks in sample Be1 have shifted to the right compared to sample Be6. This is consistent with the wettability characteristics of the samples. Also compared to the reference oil, the main peak has shifted to higher values with respect to the reference oil.

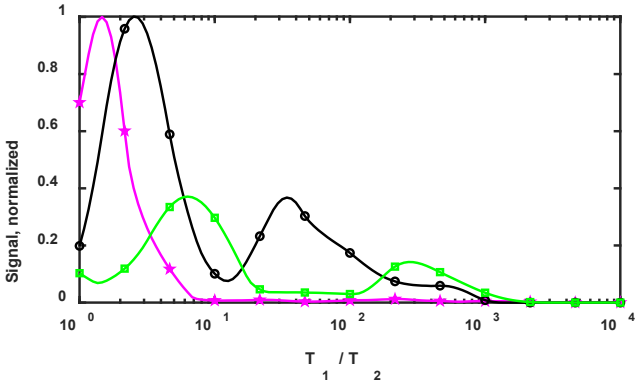

Fig. 8. Distribution of the ^{13}C T_1/T_2 ratio for Be1 (■), Be6 (●) and reference oil (*). Distributions of Be1 and Be6 are normalized with respect to the signal of Be6.

3.1.1 Validation of ^{13}C results

To validate our results based on T_2 and T_1-T_2 relaxation correlation two types of analysis were performed. The first was based on the signal intensity (Figure 9) while the second approach was based on Fig. 4 and Eq. 2 previously discussed in the theory section.

The advantage of using ^{13}C MR is that all the information is obtained directly from the oil. ^{13}C not only gives direct information of bulk and surface properties of oil but also it reveals oil content saturating the core plugs. Oil saturations of core plugs obtained by ^{13}C T_2 [13], and ^{13}C T_1-T_2 are plotted vs. S_{or} obtained by SCAL and are shown in Fig. 9. It is clearly observed that a remarkable match exists between the results, which confirms the validity of the ^{13}C measurements. It is worth noting that IR-CPMG experiments were undertaken with 32 scans, but CPMG experiments were undertaken with 512 scans. This emphasizes that the IR-CPMG experiment is substantially immune to low SNR problems. It should be mentioned that the samples were at residual oil saturation, S_{or}, which means that oil saturation is at minimum that makes the determination of oil saturation difficult.

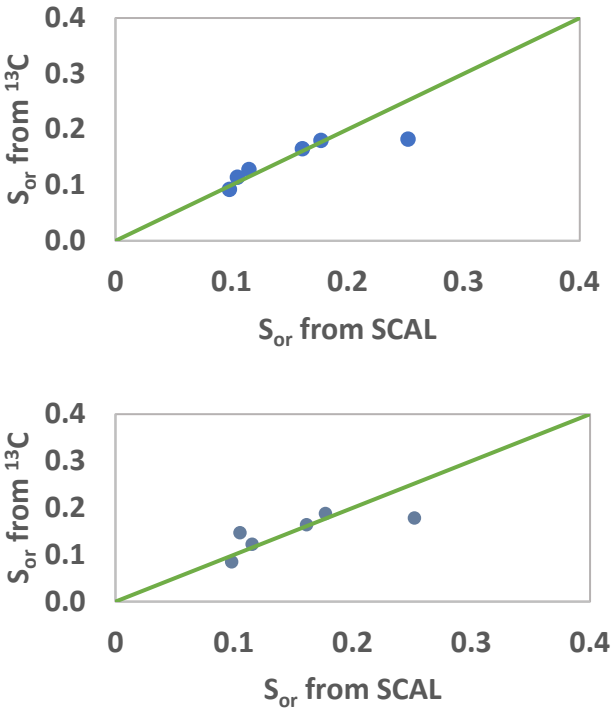

Fig. 9. S_{or} from ^{13}C MR vs. S_{or} from SCAL. In the top figure S_{or} is obtained from ^{13}C CPMG, and in the bottom figure S_{or} is obtained from ^{13}C T_1-T_2. The solid line is diagonal. All data should fall on the solid line if each method gives equal S_{or} results.

For the second kind of validation, we used the theory of T_1/T_2. Figure 10 shows the T_1/T_2 line according to Eq. 4 on top of the ^{13}C T_1-T_2 relaxation correlation for the samples. For all samples T_b = 2.5 s. The sample T_2 distribution was characterized by a single value, which aligns with measured T_1-T_2, and is physically sensible. For sample Be1 the T_{1s}/T_{2s} was chosen to be 6.6 to fit the peak. Since this sample was the reference sample, this line was plotted on all the other T_1-T_2 plots. If the peak of any other sample lies on the T_{1s}/T_{2s} = 6.6, T_b = 2.5 s line, that means that the sample had the same characteristics, same mechanism of relaxation, and bulk effects masked the surface effects. According to Fig. 10, none of the samples lie on the above-mentioned line and separate lines were plotted to fit the peaks. Peaks of samples Be2 and Be3 coincided with the T_{1s}/T_{2s} = 4 line. This means that the oil in these samples have lower surface interactions and are less oil wet. The water wet samples, Be4, Be5, and Be6 did not fall on the T_{1s}/T_{2s} = 6.6 and T_{1s}/T_{2s} = 4 lines. The peaks can be fitted by the T_{1s}/T_{2s} = 2 line for samples Be4 and Be5, and by T_{1s}/T_{2s} = 2.2 for sample Be6. With this simple analysis we have shown, and proved, that T_1/T_2 results for these samples were immune to bulk effects and corresponding values of T_1/T_2 were directly showing the T_{1s}/T_{2s}. This means that differences in oil saturation did not affect the T_1/T_2 analysis. This type of analysis cannot be conducted using T_2 analysis as it is also influenced by bulk effects coming from different saturations.

3.2 ^1H measurements

Figure 11 shows the ^1H T_2 distribution for the reference oil, sample Be1, and sample Be6. As can be seen there is no clear separation between oil and water in the ^1H T_2 distribution of samples Be1 and Be6 and signals are overlapping. Since the other samples have the same characteristics, they are not plotted.

Figure 12 shows ^1H T_1-T_2 relaxation correlation plots of the samples. According to the plots, no distinct zones of water and oil are observable, but one can detect a tail attached to a zone with high T_1 and T_2. By examining the T_1 and T_2 values of the oil and water reference samples, it is possible to determine that the zone with higher T_1 and T_2 and a higher signal amplitude belongs to the water phase, and the tail corresponds to the oil phase. The peak of the water zone is almost constant for all the samples. This can be due to high water saturation which means that bulk effects are masking the surface effects for the water phase. This means that for water wet samples which we expect higher T_1/T_2 of water, bulk effects mask the surface relaxations. Since the samples are at S_{or}, bulk relaxation does not mask the surface relaxation of oil and that is why the tail of the ^1H T_1-T_2 is shifted to the higher T_1/T_2 for oil wet samples.

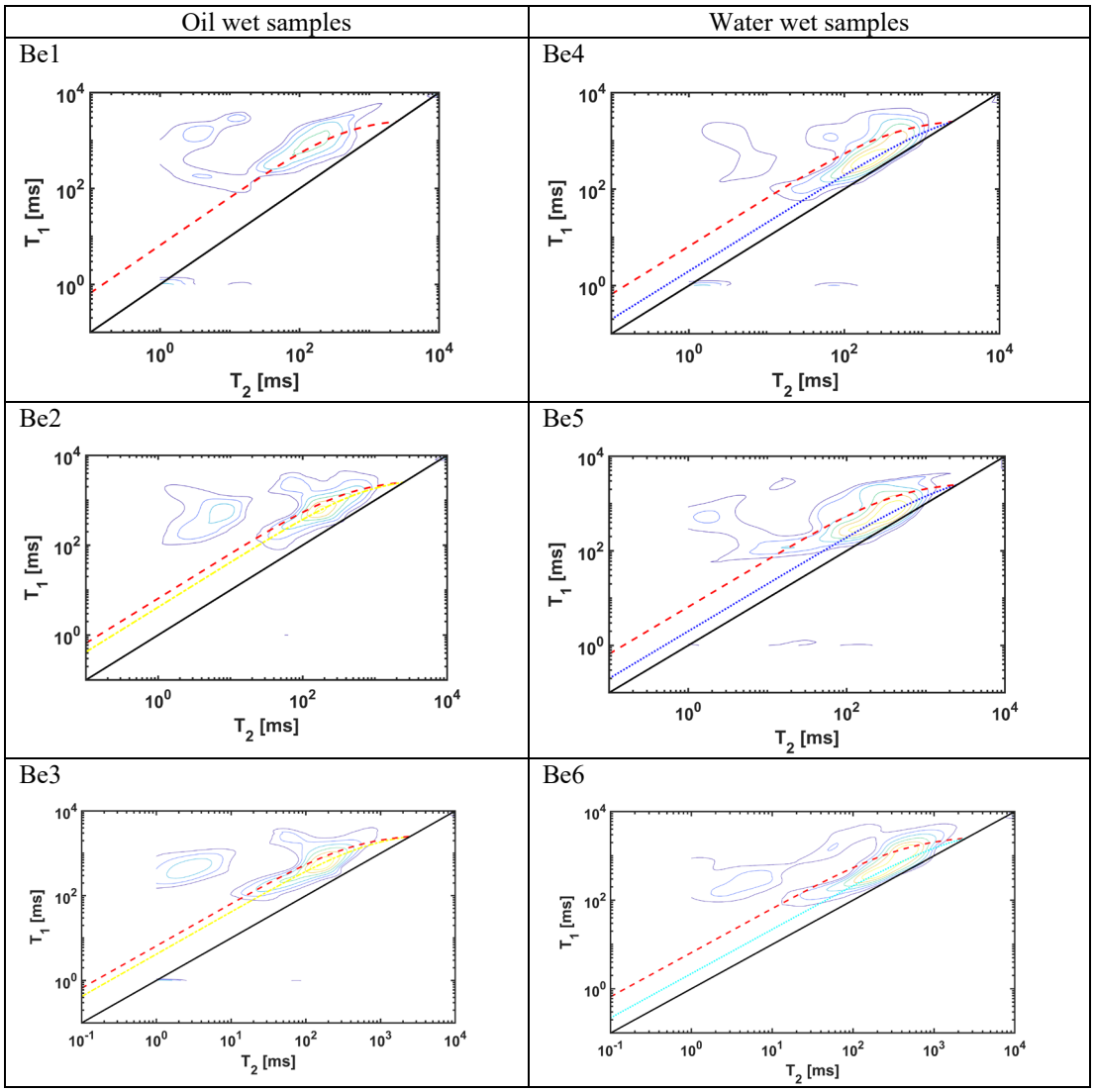

Fig. 10. ^{13}C T_1-T_2 relaxation correlation for the samples with T_1/T_2 lines. For the T_1/T_2, T_b was considered 2.5 s. For sample Be1 which was the reference sample, T_{1s}/T_{2s} was 6.6 which is shown as (– – –) and is plotted in all other plots for comparison. For samples Be2 and Be3 T_{1s}/T_{2s} was 4 and the line is shown as (– – –). For samples Be4 and Be5 T_{1s}/T_{2s} was 2 (…) and for sample Be6 T_{1s}/T_{2s} was 2.2 (…).

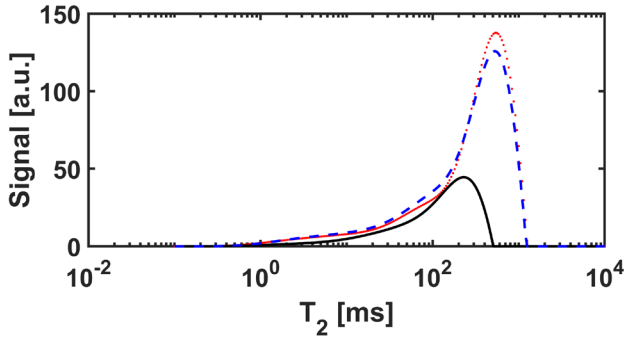

Fig. 11. ^{1}H T_2 distribution for reference oil sample (-), Be1 (…) and Be6 (- - -).

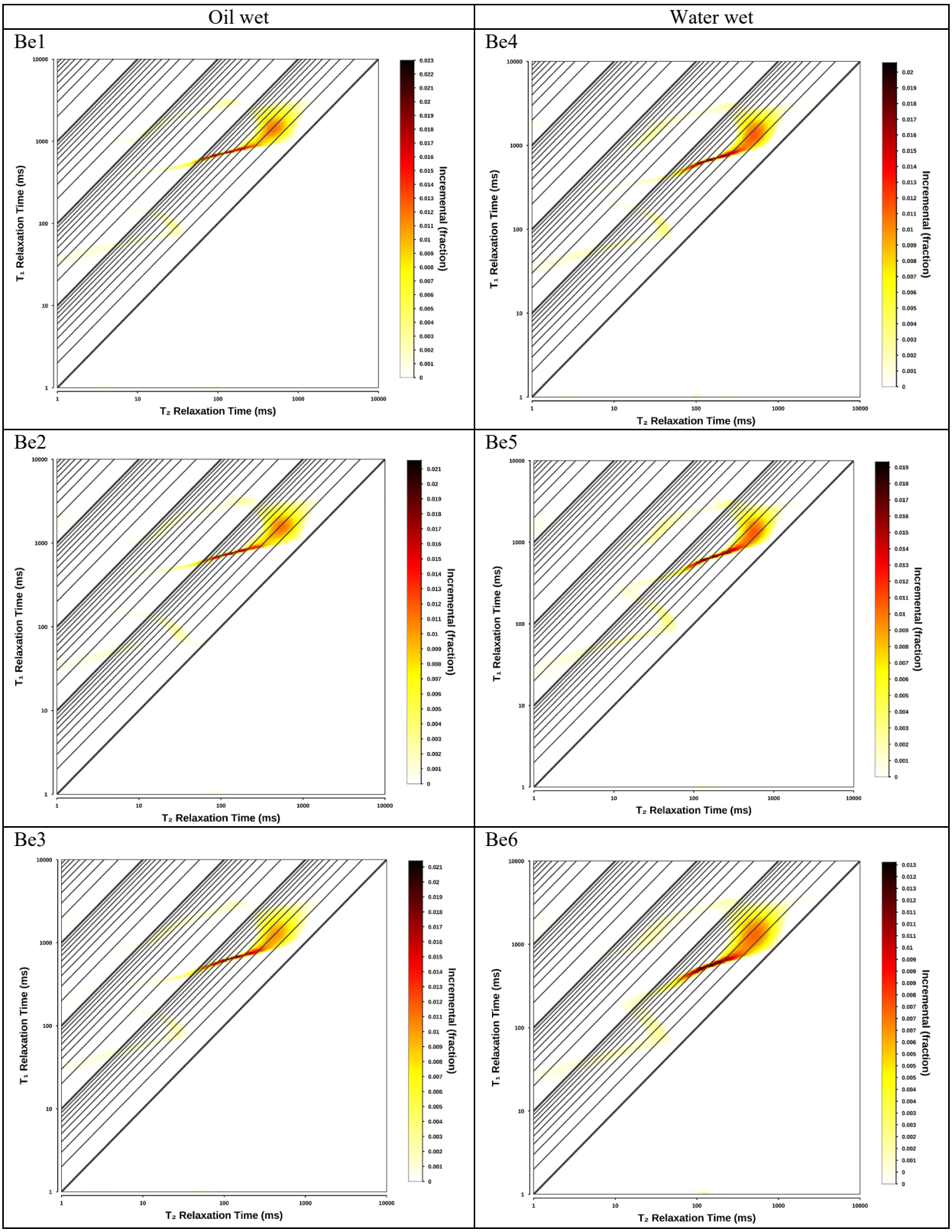

Fig. 12. ^{1}H T_1-T_2 relaxation correlation for the samples.

These results show that although ^{1}H MR data can be used for the qualitative study of surface interactions and rock wettability, it does not provide quantitative information for realistic rock samples. Furthermore, this experimental work confirmed that ^{13}C MR is a reliable new technique to study wettability of the core plugs. The main advantage of using ^{13}C is that it does not require separate T_1 and T_2 peaks for oil and water, as it directly provides information on oil phase only. Future work will focus on establishing a reliable ^{13}C MR wettability index.

4 Conclusions

Wettability determination by MR requires methods that can differentiate the phases inside the porous medium and are sensitive to surface interaction. In this paper, ^{13}C MR measurements were used to isolate signal from hydrocarbons in the samples. This method enables us to obtain hydrocarbon signal and relaxation times without the need of distinguishing phases by using unrealistic fluids. Application of this measurement will assist in reliable analyses of rock wettability, not only in conventional crude oil, but also in heavy oil with very complex MR relaxation time distributions that prevent signal differentiation.

In this paper, we utilized ^{13}C MR measurements as a valuable tool to investigate hydrocarbon properties in representative core plugs and model systems. Our study focused on obtaining information about hydrocarbon ^{13}C MR T_2 relaxation time and the T_1/T_2. The obtained results provide clear evidence of the sensitivity of ^{13}C MR measurements to surface interactions, enabling the reliable assessment of wettability characteristics.

Although ^{13}C MR has low sensitivity due to low natural abundance and low gamma, we showed that it provides accurate information on oil content. In addition, we have demonstrated that the methods utilized for wettability analysis with ^{1}H MR can also be applied to investigate ^{13}C MR, given that both nuclei have a spin of 1/2 with the unique advantage that all signal is coming from the oil.

The findings of our study have significant implications for understanding wettability in hydrocarbon rock systems. Specifically, we observed that rock samples with an oil-wet nature display a distinct behavior in their ^{13}C T_2 relaxation time. These oil-wet rock samples exhibited a reduction in the ^{13}C MR T_2 relaxation time, indicating increased interactions between the hydrocarbons and the surface. Additionally, we found that the T_1/T_2 ratio, which removes effects of pore size, was increased in oil-wet rock samples.

The ability to obtain rock wettability information through ^{13}C MR measurements represents a significant advancement in this field of research. By utilizing this technique, researchers can now work towards establishing a wettability index based on reliable measurements, providing valuable insights into the wetting behavior of hydrocarbon rock systems. This development opens new avenues for characterizing and understanding the interfacial properties of hydrocarbon reservoir formations, further enhancing our ability to optimize oil recovery processes.

This work was supported by an NSERC Alliance award grant [ALLRP 571885–21] and an NSERC Discovery grant [2022-04003]. The authors thank TotalEnergies and Green Imaging Technologies for financial support.

References

1. J.E. Bobek, C.C. Mattax, M.O. Denekas, Trans. AIME **213**, 155–160 (1958). https://doi.org/10.2118/895-G.
2. Y.-Y. Quan, L.-Z. Zhang, R.-H. Qi, R.-R. Cai, Sci. Rep. **6**, 38239 (2016). https://doi.org/10.1038/srep38239.
3. S. Moradi, N. Hadjesfandiari, S.F. Toosi, J.N. Kizhakkedathu, S.G. Hatzikiriakos, ACS Appl. Mater. Interfaces. **8**, 17631–17641 (2016). https://doi.org/10.1021/acsami.6b03644.
4. S.K. Woche, M.-O. Goebel, R. Mikutta, C. Schurig, M. Kaestner, G. Guggenberger, J. Bachmann, Sci. Rep. **7**, 42877 (2017). https://doi.org/10.1038/srep42877.
5. M.T. Tweheyo, T. Holt, O. Torsæter, J. Pet. Sci. Eng. **24**, 179–188 (1999). https://doi.org/10.1016/S0920-4105(99)00041-8.
6. Y.C. Chang, K.K. Mohanty, D.D. Huang, M.M. Honarpour, J. Pet. Sci. Eng. **18**, 1–19 (1997). https://doi.org/10.1016/S0920-4105(97)00006-5.
7. Else Johannesen, J. Howard, A. Graue, SCA (2008).
8. M. Kumar, T. Senden, M.A. Knackstedt, S.J. Latham, R.M. Sok, A.P. Sheppard, M.L. Turner, V.L. Pinczewski **50** (2009).
9. L. Hendraningrat, O. Torsæter **28**, 6228–6241 (2014). https://doi.org/10.1021/ef5014049.
10. Z. Aghaeifar, S. Strand, T. Puntervold **33**, 3989–3997 (2019). https://doi.org/10.1021/acs.energyfuels.9b00023.
11. A. Valori, G. Hursan, S.M. Ma, PETROPHYSICS **58**, 352–365 (2017).
12. A. Valori, B. Nicot, PETROPHYSICS **60**, 255–263 (2019). https://doi.org/10.30632/PJV60N2-2019a3.
13. N. Ansaribaranghar, M.S. Zamiri, L. Romero-Zerón, F. Marica, A. Ramírez Aguilera, D. Green, B. Nicot, B.J. Balcom (Eds.). International Symposium of the Society of Core Analysts, SCA2023-005, 2023.
14. N. Ansaribaranghar, M.S. Zamiri, L. Romero-Zerón, F. Marica, A. Ramírez Aguilera, D. Green, B. Nicot, B.J. Balcom (Eds.). International Symposium of the Society of Core Analysts, SCA2023-018, (2023).
15. S.A. Criollo, Water and surfactant flooding at different wettability conditions.
16. E. Amott **216**, 156–162 (1959). https://doi.org/10.2118/1167-G.
17. V. Arekhov, R.E. Hincapie, T. Clemens, M. Tahir **12** (2020). https://doi.org/10.3390/polym12102241.
18. Y. Han, K. Liu **35**, 14734–14745 (2021). https://doi.org/10.1021/acs.energyfuels.1c02301.

19. M.A. Fernø, M. Torsvik, S. Haugland, A. Graue, Energy Fuels. **24**, 3950–3958 (2010). https://doi.org/10.1021/ef1001716.
20. M. Mascle, S. Youssef, H. Deschamps, O. Vizika, PETROPHYSICS **60**, 514–524 (2019). https://doi.org/10.30632/PJV60N4-2019a5.
21. M. Tahir, R.E. Hincapie, N. Langanke, L. Ganzer, P. Jaeger **12** (2020). https://doi.org/10.3390/polym12061227.
22. H. Ehtesabi, M.M. Ahadian, V. Taghikhani, M.H. Ghazanfari, Energy Fuels. **28**, 423–430 (2014). https://doi.org/10.1021/ef401338c.
23. G. Li, X. Yi, Y. Zhang, Y. Li, J. Surfactants Deterg. **26**, 195–203 (2023). https://doi.org/10.1002/jsde.12627.
24. L. Yuan, Y. Zhang, H. Dehghanpour **35**, 7787–7798 (2021). https://doi.org/10.1021/acs.energyfuels.1c00001.
25. F. Pairoys, C. Caubit, L. Rochereau, A. Nepesov, Q. Danielczick, N. Agenet, F. Nono (Eds.). International Symposium of the Society of Core Analysts, SCA2023-007, 2023.
26. Y.-Q. Song, L. Venkataramanan, M.D. Hürlimann, M. Flaum, P. Frulla, C. Straley, J. Magn. Reson. **154**, 261–268 (2002). https://doi.org/10.1006/jmre.2001.2474.
27. J. Mitchell, T.C. Chandrasekera, L.F. Gladden, Prog. Nucl. Magn. Reson. Spectrosc. **62**, 34–50 (2012). https://doi.org/10.1016/j.pnmrs.2011.07.002.
28. K.M. Song, J. Mitchell, H. Jaffel, L.F. Gladden, J. Mater. Sci. **45**, 5282–5290 (2010). https://doi.org/10.1007/s10853-010-4572-7.
29. S. Vashaee, M. Li, B. Newling, B. MacMillan, F. Marica, H.T. Kwak, J. Gao, A.M. Al-harbi, B.J. Balcom **287**, 113–122 (2018). https://doi.org/10.1016/j.jmr.2018.01.001.
30. H.Y. Carr, E.M. Purcell **94**, 630–638 (1954). https://doi.org/10.1103/PhysRev.94.630.
31. S. Meiboom, D. Gill **29**, 688–691 (1958). https://doi.org/10.1063/1.1716296.
32. J.G. Seland, M. Bruvold, H. Brurok, P. Jynge, J. Krane **58**, 674–686 (2007). https://doi.org/10.1002/mrm.21323.
33. J. Mitchell, E.J. Forham, Rev. Sci. Instrum. **85** (2014). https://doi.org/10.1063/1.4902093.
34. R. Freedman, S. Lo, M. Flaum, G.J. Hirasaki, A. Matteson, A. Sezginer **6**, 452–464 (2001). https://doi.org/10.2118/75325-PA.
35. W.J. Looyestijn, J. Hofman **9**, 146–153 (2006). https://doi.org/10.2118/93624-PA.
36. M.D. Hürlimann, Y.-Q. Song US Patent 8,362,767 B2, (2013).
37. J. Mitchell, L.M. Broche, T.C. Chandrasekera, D.J. Lurie, L.F. Gladden **117**, 17699–17706 (2013). https://doi.org/10.1021/jp405987m.
38. J. Mitchell, T.C. Chandrasekera, D.J. Holland, L.F. Gladden, E.J. Fordham **526**, 165–225 (2013). https://doi.org/10.1016/j.physrep.2013.01.003.